Invited Talk presented at the SLAC Topical Conference on Strong Interactions, August 1974 .

FERMILAB-CONF-74-153 #14

File Copy

CONF-74-153-1
E-0014

(4)

# Proton-Proton Inelastic Scattering at FNAL

P. FRANZINI

Columbia University, New York, N.Y.

Research supported by the National Science Foundation.

## I. INTRODUCTION

Because of the great complexity of hadron interactions at high energy, it becomes necessary to seek new ways to study high energy collisions. One way is to concentrate on the observation in the final state of one of the initial particles. The first such reaction to be studied at a proton accelerator is of course $p+p \to p+ \ldots$, often written as $p + p \to p + X$, where X stands for everything other than the observed proton in the final state. If the information contained in the internal variables of X is ignored then the reaction $p + p \to p + X$ is uniquely defined in terms of three variables, usually chosen to be the three lorentz invariant quantities s (total c.m. energy squared), t (square of the 4-momentum transfer from initial to final proton) and $M_X^2$ (the magnitude squared of the sum of the 4-momenta of all particles in X). A new range in s has been opened up by the NAL accelerator and the CERN ISR. For a given s, we have: $m_p^2 < M_X^2 \leq s$ and $0 < -t \leq 2s$ with $-t \geq M_X^4/s^2$ (we use $m_p \cong 1$ (GeV)$^2$).

FERMILAB-CONF-74-153-E

Extremely limited knowledge was available until very recently about the mass spectrum of X and about the t dependence of the cross section. In other words, very little knowledge was available about the form of the doubly differential cross section $d^2\sigma/dtdM_X^2$, nor its energy dependence. Some first results were obtained at the ISR[1] but with extremely poor mass squared and t resolution. Also those results were obtained for $-t \geqslant 0.3$ $(GeV/c)^2$ while the bulk of the cross section occurs at $-t \leqslant 0.3$ $(GeV/c)^2$. Preliminary results with much better resolution were obtained[2] by FNAL Experiment E-14 at 300 GeV for low $M_X^2$ values and some information came from the Rutgers-Imperial College[3] experiment at FNAL at various energies.

We shall present, in the following, the results of a much improved experiment performed at the Internal Target Area over the energy range 100-400 GeV (E-221) as well as comment on the results of an attempt to extract information on p-p inelastic scattering from p-d scattering, FNAL experiment E-186. Experiment E-221 was performed by P. Franzini and S. Childress of Columbia University and by J. Lee-Franzini, R. McCarthy and R.D. Schamberger of SUNY at Stony Brook. The results reported here are from a preliminary analysis of the data. Many minor corrections have not been taken into account and often results will be presented in "arbitrary units" rather than mb. This does not in any way affect the

FERMILAB-CONF-74-153-E

conclusions drawn. E-186 was performed by the Dubna-NAL-Rochester-Rockefeller Collaboration and the results quoted in the following were presented at the London International Conference in High Energy Physics.

At very high energy, the reaction $p + p \rightarrow p + X$ is best studied at small t and for $M_X^2 < 0.1$ s by detecting the recoil of the target proton rather than trying to measure a very small change in momentum and direction of the beam proton. Typically a t value of $-0.1$ $(GeV/c)^2$ corresponds to a scattering angle of the fast proton at 300 GeV, of $10^{-3}$ rad and a 5% accuracy in t requires an accuracy in $\theta$ of $5 \times 10^{-5}$ rad. Similarly, a mass squared accuracy of 0.5 $(GeV)^2$ requires at 300 GeV an accuracy in momentum measurement of $\pm$ 0.08%. If instead one observes the recoil proton then $t = 2m_pT$ where T is the kinetic energy of the proton and $M_X^2 = m_p^2 - 2m_pT - 2E_{in}T + 2p_{in}p_r\cos\theta$ from which $\delta t/t = \delta T/T$ and $\delta M_X^2 \approx 2pp_r\delta\theta$. In other words, a 5% accuracy in t requires the same accuracy in the measurement of the recoil energy and an accuracy of $2 \times 10^{-3}$ rad gives an error in mass squared somewhere around 0.1 $(GeV)^2$. In addition, the recoil angle is very large (up to $\approx 90^o$) therefore facilitating the measurement. Of course while the relative accuracy required is much more modest, the range of the variables is much larger. In addition, one is faced with the strange problem in high energy physics of measuring

FERMILAB-CONF-74-153-E

kinetic energies in the range 5 to 100 MeV if one wants to explore the t range of -0.01 to -0.2 $(GeV/c)^2$ where the bulk of the cross section is located.

## II. EXPERIMENTAL METHOD

### A. Energy Measurement

Energies of a few MeV are commonly measured in Nuclear Physics experiments by stopping the particle in a thick semiconductor layer, depleted of charge carriers by the application of a suitable reverse bias. The charge collected after passage of a particle is proportional to the energy lost in the semiconductor. We shall from now on refer to the charge collected as the energy E lost in the detector. Solid state detectors can measure proton kinetic energies up to 30 MeV with accuracy typically of $\pm$ 0.05 MeV. The problem with measuring higher energies is simply due to the tremendous difficulties (and cost) connected with growing silicon crystals thick enough to stop protons of 100 MeV or more kinetic energy.

As we shall discuss later, we use for targets $CH_2$ and C, and obtain the proton cross section from subtracting the two distributions. This however requires the identification of the particles detected since a large number of nuclear fragments ($H_2$, $H_3$, $He_3$, $He_4$, etc.) are produced in p-C collisions. We therefore use telescopes consisting of 3 detectors. See Fig. 1. The first detector is very thin

(150 μ) and has charge collection electrodes deposited only on a small fraction of its area. These electrodes are rectangular, 4 x 6 $mm^2$ deposited over a Si slice of 150 $mm^2$ area. This detector defines the solid angle and acts as a collimator to accept only particles crossing the center of the following detectors of the telescope. We had previously used tungsten collimators which caused problems with particles hitting their edges. A coincidence between the first detector and the second one of medium thickness (1000 μ) is required. The third detector is 5000 μ thick. The charge collected from all the detectors is stored in analog form for each coincidence between the first two detectors. The correlation between $E_1$ and $E_2$ or $E_2$ and $E_3$ allows us to identify particle type for stopping particles. The correlation between $E_2$ and $E_3$ allows us to also determine the kinetic energy for protons fast enough to cross the third counter. A sketch of the above mentioned correlations is given in Fig. 2. Figure 3 gives an actual scatter plot of $E_2$ vs $E_3$ for events produced by 300 GeV protons in C and $CH_2$ targets. The energy of a proton stopping in the second detector is given at the entrance into the second detector by $T = E_2$. For protons stopping in the third detector, we have $T = E_2 + E_3$. Finally, for a proton crossing the third detector we still can determine its energy. The following is an approximate example:
The range energy relation is approximately given by
$T = \frac{a}{M} R^{1.7}$ .

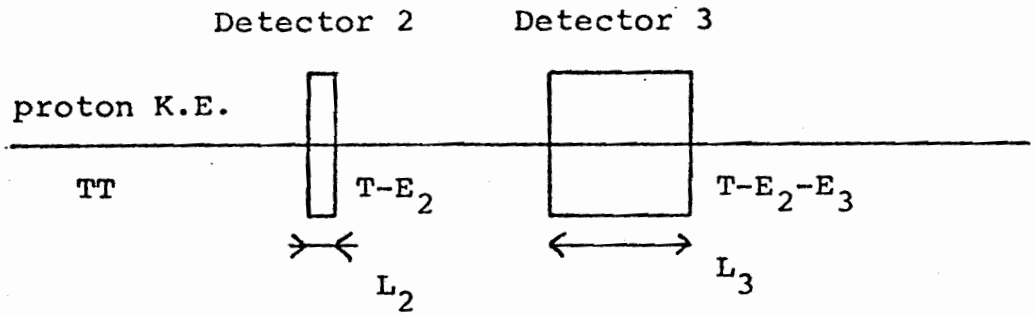


Let R' be the residual range, then

$$\frac{a}{M} T^{1.7} - L_2 - L_3 = R' = \frac{a}{M}(T-E_2-E_3)^{1.7} \text{ or}$$

$$T^{1.7} = (T-E_2-E_3)^{1.7} + \frac{M}{a}(L_2 + L_3) \quad .$$

This equation cannot be solved in closed form for T but of course it can be solved numerically and stored in a table. Similarly for a particle stopping in detector 3, we can solve for the mass

$$M = \frac{a}{L_2}\left[(E_1+E_2)^{1.7} - E_2^{1.7}\right] \quad .$$

In this way, we are able to measure proton kinetic energy up to about 130 MeV with reasonable accuracy ($\leq$ 5%) using a total thickness of 6150 μ of Si. It should be noted that this extension of a traditional method has never been used before. Otherwise 68,000 μ of Si would have been necessary to stop a proton of 130 MeV. All energy measurements as defined here require correction for losses in detector number 1.

FERMILAB-CONF-74-153-E

## B. Target

The target as briefly mentioned consisted of a wheel spinning at 65 Hz, on which carbon and polypropelene fiber are mounted. Polypropelene $(CH_3\text{-}CH = CH_2)_n = (CH_2)_n$ rather than polyethelene (also $(CH_2)_n$) was used because of the former's superior strength and higher melting point ($\leqslant 200^\circ$ C). Still, because of the high intensity of the internal beam at NAL ($\leqslant 5 \times 10^{17}$ proton/sec), the poly fibers would vaporize in a fraction of a second if fully inserted in the beam. The tips of the fibers were brought into the periphery of the beam and kept at the appropriate height by a "servo" measuring the beam target interaction rate.

The normalization of the C data to the $CH_2$ data is performed by counting the total number of identified stopping deuterons and tritons for both targets. Since this is done with the same detectors which are used for detecting protons, one obtains the proper product (effective beam intensity) x (No. of C atoms) for each target without having to independently measure beam intensity, dead time and number of C atoms for each target.

## C. Angle Measurement

To cover a significant range in $M_X^2$, it is necessary to cover the angular range $50^\circ$ to $85^\circ$ while maintaining a good angular resolution. We mounted 8 telescopes on a carriage which moves on a circular track whose center is the interaction

point. The distance between the front detector and the interaction point is 850 mm, thus giving an angular resolution of $\sim \pm 2.5$ mr. The angular separation between telescopes is $2.4^{\circ}$. The array thus spans $\sim 17^{\circ}$. To cover the angles in between the telescopes as well as to cover a large angular range the detector carriage is moved to a new position typically every hour.

D. Data Reduction

In order to obtain significant information on $d^2\sigma/dtdM_X^2$ at many energies as well as t and $M_X^2$ values, it is necessary to collect of the order of $\sim 10^9$ triggers because of the large increase in statistical error due to the subtraction of C data from $CH_2$ data. If each event were recorded with the appropriate information on tape, this would require i) writing of the order of 1000 tapes, ii) process these tapes through a computer to identify particle type and compute recoil energies, iii) histogram events as dN/dT for each telescope, iv) compute the normalization and the subtraction, v) transform $d^2N/d\theta dT$ into $d^2N/dtdM_X^2$ or $d^2\sigma/dtdM_X^2$. Of these points i) is both unpleasant and limits the data taking rate to the amount of memory available; ii) is however the most serious disadvantage. In order to compute mass and energy as shown before and reduce the data to dN/dT for each telescope requires 1 msec of CPU time per event in a modern general purpose computer such as CDC 6600. We therefore built a special purpose computer to perform all the algebra shown previously. The main philosophy

FERMILAB-CONF-74-153-E

in the design of this computer is to have a memory containing tables of $E_2$ vs $E_3$ for various particle types (tritons, deuterons, stopping protons, crossing protons) as well as T vs $E_3$ for crossing protons. Also all the arithmetics are executed by individual elements instead of recirculating data through the same arithmetic unit. Finally, particle recognition and kinetic energy calculation are performed in parallel. See Fig. 4. While learning to use such a device which we call an "event analyzer", we came to realize that not only we saved ourselves months and months of work on a general purpose computer, but that a hard wired special purpose computer with large memory is more easily modified than a program. In particular, during a few months we transferred all the display and monitoring functions from the PDP-11 to the "event analyzer". This is done by physically adding new functions to the analyzer and thus never interferes nor slows down the event flow as is the case for a general purpose computer. The "event analyzer" output, in the run mode, is a single 16 bits word which represents the kinetic energy of the recoil, the telescope number or angle, the beam energy as defined by 8 gates during the acceleration ramp and whether the target is C or $CH_2$. This word is used to address and increment by 1 a memory location in the PDP-11. Thus, one directly accumulates in memory a long string of histograms of dN/dT for different angles, energies and targets.

FERMILAB-CONF-74-153-E

The processing time for an event varies between 156 and 496 ns. The memory contents are dumped onto tape typically every $\sim 10^6$ triggers to minimize losses due to malfunctions. The net result is that i) $\sim 5 \times 10^8$ triggers correspond to one full tape; ii) the algebra and histogramming have been performed on line without any loss of time.

E. Calibration and Checks

In reality, we do not use the range energy relation given previously, but we do instead calibrate our energy scale and the $E_2$ vs $E_3$ correlation by using the data themselves. The $E_2$ vs $E_3$ correlation is obtained directly from scatter plots as shown in Fig. 3. The final scale calibration is performed by moving each telescope to appropriate angles and observing the elastic scattering peaks whose energies are known from angle. The angle is measured remotely with an encoder to 0.3 mr. This calibration is performed for each telescope to account for small differences in thickness and/or amplifier gain and checked continuously.

F. Resolution in Mass Squared

At sufficiently low energies the elastic peak becomes completely separated from the inelastic continuum. A very short run at 55 GeV gave the result shown in Fig. 5. We observe a sharp peak in the cross section at $M_X^2 = m_p^2$ and the peak is symmetric. The peak is well fitted by a gaussian with $\sigma = 0.014\ (\mathrm{GeV})^2$. At higher energies, $\sigma$ increases as E and the elastic peak merge with the inelastic continuum.

FERMILAB-CONF-74-153-E

In all cases, the elastic peak falls, for $M_X^2 < m_p^2$, by more than three orders of magnitude and well below the inelastic signal. We therefore simply subtract the left side of the measured elastic peak from the right side to obtain the inelastic cross section. Typical data are shown in Fig. 6 at 300 GeV. The cross section with the elastic peak subtracted is shown in Fig. 7.

## III. PHYSICS RESULTS

Before discussing the physics result, we mention one last check. Directly from the finally computed $d^2\sigma/dtdM_X^2$, one can obtain the cross section $d\sigma/dt$ integrated over the prominent peak at the proton mass, i.e., the t dependence of the elastic cross section. This is shown in Fig. 8 together with fits to the form $e^{bt}$. Values for b are given in Fig. 8. The very good agreement with reported values is a check on our ability to correctly measure the t dependence. In addition, these data are used to transform all our measurements to absolute units.

Typical results for the inelastic cross section are shown in Fig. 9. Here $d^2\sigma/dtdM_X^2$ for beam energy of 300 GeV is plotted versus $M_X^2$ for two narrow t bands centered around $-t = 0.066$ and $-t = 0.122$. A similar plot is shown in Fig. 10 for a beam energy of 395 GeV, for another two different values of t. Here the vertical scale is arbitrary. A large number of such plots were obtained for incident energies

FERMILAB-CONF-74-153-E

of 120, 200, 300, 395 GeV. A common property of all the mass spectra is the extremely fast drop off of the cross section for masses squared up to 15 to 20 $(GeV)^2$ followed by a long plateau up to the end of the measured range. The shape of the cross section suggests a dependence of the type $a(t) + b(t)/M_x^{\alpha}$. We have fitted all our data to this form and obtained values of $\alpha$ around 4 for all values of E and t. Four such fits are shown in Figs. 9 and 10. The value of the cross section for the plateau at large masses decreases, at fixed t, with increasing incident energy while the low mass cross section is energy independent. All of our data are thus consistent with a form of the type $d^2\sigma/dtdM_X^2 = a(t)/s + b(t)/M_X^4$. In this formula a(t) and b(t) are energy independent to a 20% accuracy.

To obtain the t dependence of the a and b coefficients does require however more accuracy than at present is available because of the factor $1/M_X^4$. At the moment, it appears that the data are consistent with a and b having the same general t dependence, approximately $e^{8t}$ for -t less than 0.1 and $e^{6t}$ for $-t > 0.1$ $(GeV/c)^2$. This is in excellent agreement with many experiments[1,3,4] which all have reported that for $-t \geqslant 0.1$, the slope is typically 5 to 6, except for $M_X^2 \approx 2$ $(GeV)^2$ where the slope[1,5] is 18 as is also observed in the present experiment.

The shape of the mass spectrum is however in contradiction with other reported results.[1,6] One of these

FERMILAB-CONF-74-153-E

experiments was performed with colliding beams and reported a mass resolution of $\sim 10\ (\mathrm{GeV})^2$. Folding the $10\ (\mathrm{GeV})^2$ resolution into our spectra does indeed produce a much shallower rise toward low masses and brings the ISR result in agreement with us.

## IV. COMPARISON WITH E-186

An experiment with resolution comparable to ours ($\delta M_X^2$ typically twice as large as ours) has been performed by the U.S.-U.S.S.R. Collaboration at NAL.[6] Their experiment detects, in a fashion similar to ours, deuteron recoils from p-d interactions. In this way, the cross section for $p + d \rightarrow d + X$ is obtained. The assertion is made that by dividing the measured cross section by the "deuteron form factor" one can obtain the cross section for $p + p \rightarrow p + X$. Explicitly, they write

$$\left.\frac{d^2\sigma}{dtdM_X^2}\right]_{pp\rightarrow pX} = \frac{1}{\left[\frac{\sigma_{tot}^{pd}}{\sigma_{tot}^{pp}}\right]^2 e^{bt+ct^2}} \left.\frac{d^2\sigma}{dtdM_X^2}\right]_{pd\rightarrow dX}$$

where the ratio of the total cross sections has been squared to account for the presumed coherence of inelastic scattering from bound deuterons. In numbers, the formula becomes

$$\left.\frac{d^2\sigma}{dtdM_X^2}\right]_{pp\rightarrow pX} = \frac{1}{3.5e^{26t+60t^2}} \left.\frac{d^2\sigma}{dtdM_X^2}\right]_{pd\rightarrow dX} .$$

Their main conclusion after performing such manipulation is that $M_X^2\ (d^2\sigma/dtdM_X^2)$ varies with incoming energy by less than 10% and is constant with mass except for the very low

FERMILAB-CONF-74-153-E

mass region. Integrating over t the above cross section by using the measured points and assuming $d\sigma/dt \approx e^{5.5t}$ for all $M_X^2 \geqslant 6(\mathrm{GeV})^2$, see Fig. 11, they obtain the results shown in Fig. 12. This result is in direct contradiction with the spectrum observed in our experiment at all t values and energies. Whether the shape of the spectrum is $1/M_X^2$ or some other form has relevance with respect to the observed rise of the total cross section as well as with respect to Regge phenomenology.[7] According to the latter if the low t cross section were dominated by a triple pomeron coupling, it would indeed show a mass dependence like $1/M_X^2$. Other triple Regge couplings give terms in $M_X$ like $1/M_X^3$ or constant. With respect to the rising cross sections a contribution of the form $1/M_X^2$ to the spectrum gives a logarithmically increasing contribution to the cross section. In fact if, $d\sigma/dM^2 \approx 0.7\ \mathrm{mb}/M^2$, then

$$\int_{3(\mathrm{GeV})^2}^{0.1s} \frac{d\sigma}{dM^2}\, dM^2 = 0.7[\ln s - 3.4]$$

(The same logarithmic increase appears for any integral from a fixed mass to a constant fraction of the phase space.) The integration limits are chosen here to cover the t and $M_X^2$ regions where we have actual measurements. Over the range $225 < s < 741\ (\mathrm{GeV})^2$ the above formula gives an increase for the cross section from 1.41 mb to 2.24 mb. An actual integration of all measured points gives, as shown in Fig. 13, a constant cross section of 1.82 mb

FERMILAB-CONF-74-153-E

with an rms fluctuation of the four measured values of 0.03 mb, each value being determined to $\sim \pm 0.04$ mb. We therefore conclude by direct measurement that we observe no increase in the diffractive portion (low $M^2$, low t) of the inelastic cross section, contrary to the formula quoted by the U.S.-U.S.S.R. Collaboration. Moreover, the value 1.82 mb is obtained from integrating over a limited t range. A complete integration in t would double the above value. Therefore, we disagree in absolute value of the cross section as well. It might be noted that the proposed dependence for the cross section $a/s + b/M^4$ agrees quite well with the character of the cross section observed in the bubble chamber at 100 and 400 GeV by the Rochester-Michigan Group.[4] We have integrated their cross section and found the values in agreement with us.

## REFERENCES


1 M.G. Albrow et al, Nucl. Phys. B54, 6 (1973) and B51, 388 (1973).

2 S. Childress et al, Phys. Rev. Lett. 32, 389 (1974).

3 K. Abe et al, Phys. Rev. Lett. 31, 1527 (1973).

4 There are four bubble chamber exposures of 100, 200, 300 and 400 GeV protons. For a review, see D.W.G.S. Leith, Proceedings of the 1973 Meeting of the Division of Particles and Fields of the APS, 326 (1973). The 100 and 400 GeV data are reported in J. N. Chapman et al, Phys. Rev. Lett. 32, 257 (1974).

5 U.S.-U.S.S.R. Collaboration, private communication.

6 U.S.-U.S.S.R. Collaboration, NAL Experiment E-186, result presented at the NAL Seminar and the London International Conference - Preprint NAL-Conf. 74/56-Exp.

7 C.E. Detar et al, Phys. Rev. Lett. 26, 675 (1971); H.D.I. Abarbanel et al, Phys. Rev. Lett. 26, 937 (1971).

# FIGURE CAPTIONS

Fig. 1 Experimental setup and detail of one telescope. The distance from the interaction point of the NAL internal beam with the fibers to the first detector is ~ 85 cm.

Fig. 2a $E_1$ vs $E_2$ for protons, deuterons and tritons.

2b $E_2$ vs $E_3$ for protons, deuterons and tritons. Along the correlation curve for protons, values for the kinetic energy T of protons are indicated. Branch 1 in Fig. 2a corresponds to branch 1 in Fig. 2b while branch 2 corresponds to branches 2a and 2b.

Fig. 3 Scatter plot of $E_2$ vs $E_3$ for actual events. The upper two bands correspond to $D_2$ and $T_3$ fragments. The third band folding back toward the origin is produced by protons stopping in the third detector for the upper branch and crossing for the lower branch. Pions are just visible above the background.

Fig. 4 Block diagram of the event analyzer. The boxes labelled - $T(E_2)$ through $E_1$ proton down - are 25 ns memories all addressed simultaneously by the energy value $E_2$ and appropriately selected by the control. Only the output path corresponding to the case of a proton crossing all detectors is shown. Since this is the most probable case, it

Fig. 4 cont'd is tried first by the event analyzer. The propagation delays through each element are given. Note here $E_2 = E_3$ in text and $E_1 = E_2$ in text.

Fig. 5 Elastic peak and inelastic cross section at 55 GeV incident energy.

Fig. 6 Elastic peak and inelastic cross section at 300 GeV.

Fig. 7 Inelastic cross section at 300 GeV for very low $M_X^2$ after subtraction of the elastic peak.

Fig. 8 Semilog plot of the p-p elastic scattering cross section. The slope parameter is the coefficient b obtained from fitting a function $e^{bt}$ to the data.

Fig. 9 $d^2\sigma/dtdM_X^2$ vs $M_X^2$ for 300 GeV incident energy and for two t values. Also shown are fits to data of the form $a + b/M^\alpha$ with a, b, and $\alpha$ free parameters.

Fig. 10 $d^2\sigma/dtdM_X^2$ vs $M_X^2$ for 395 GeV incident energy. Also shown are fits to the data as in Fig. 9.

Fig. 11 Slope parameter for $p+p \rightarrow p+X$ as obtained by subtracting 26 from the slope measured for $p+d \rightarrow d+X$.

Fig. 12 The plotted points are supposed to represent the cross section $(d\sigma/dM_X^2)M_X^2$ for the reaction

Fig. 12 cont'd $p+p \rightarrow p+X$ and are obtained from measurements of $d^2\sigma/dM_X^2 dt$ for $p+d \rightarrow d+X$ as explained in the text. This data is used to conclude that

$$\left.\frac{d\sigma}{dM^2}\right)_{pp\rightarrow pX} \approx \frac{0.7}{M_X^2}$$ , independently of energy.

Fig. 13 Energy dependence of the integral of the measured cross section over the t range $0.023 < -t < 0.163$ and over a constant fraction of the mass spectrum, $3 < M_X^2 < 0.1\ s$ .

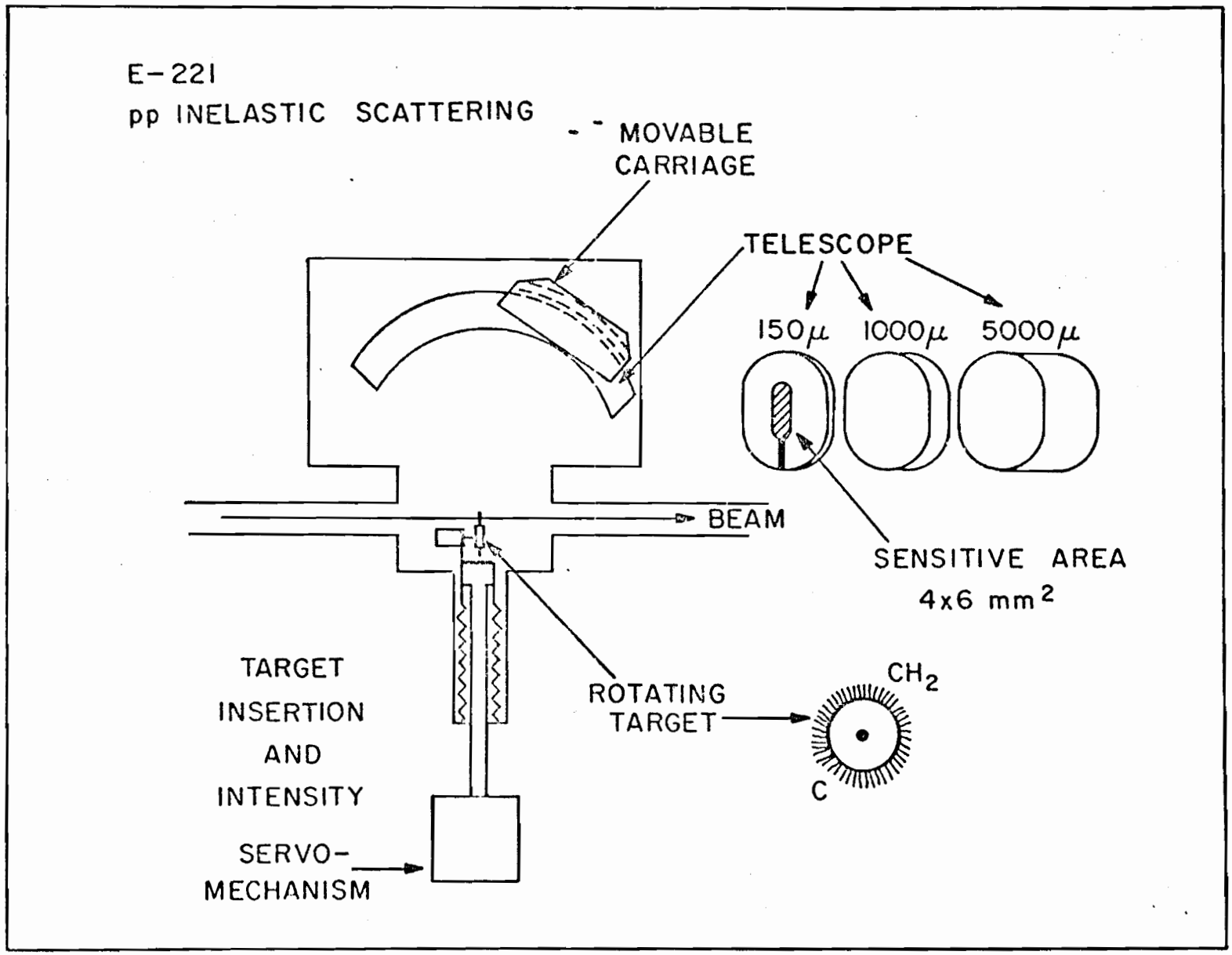
E-221
pp INELASTIC SCATTERING
MOVABLE CARRIAGE
TELESCOPE
150μ
1000μ
5000μ
BEAM
SENSITIVE AREA
4x6 mm²
TARGET INSERTION AND INTENSITY
SERVO-MECHANISM
ROTATING TARGET
CH2
C

FIG. 1

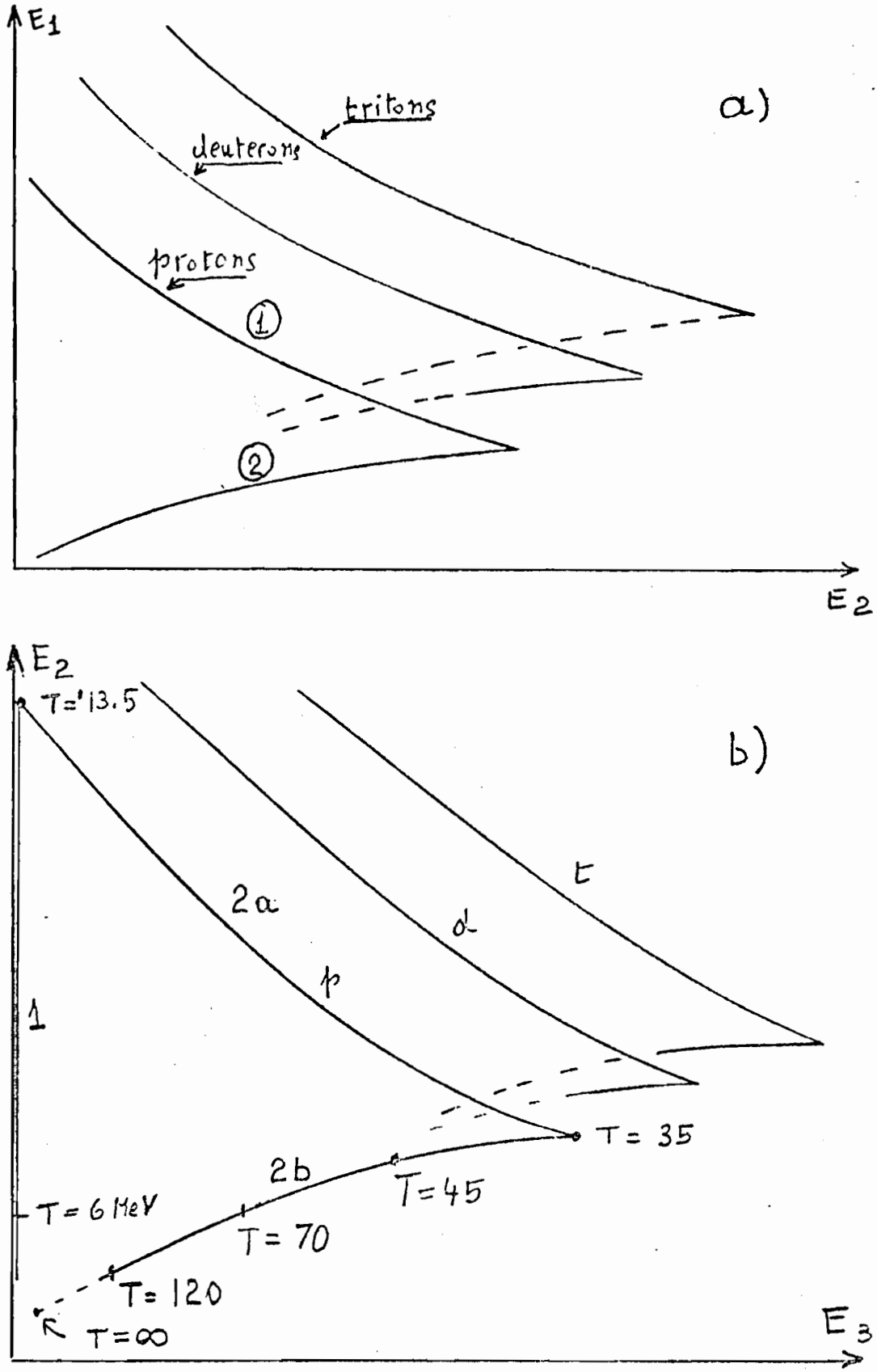
E1
tritons
deuterons
protons
a)
1
2
E2
E2
T=13.5
b)
t
2a
d
p
1
T = 35
2b
T=45
T = 6 MeV
T = 70
T= 120
T=∞
E3

FIG. 2

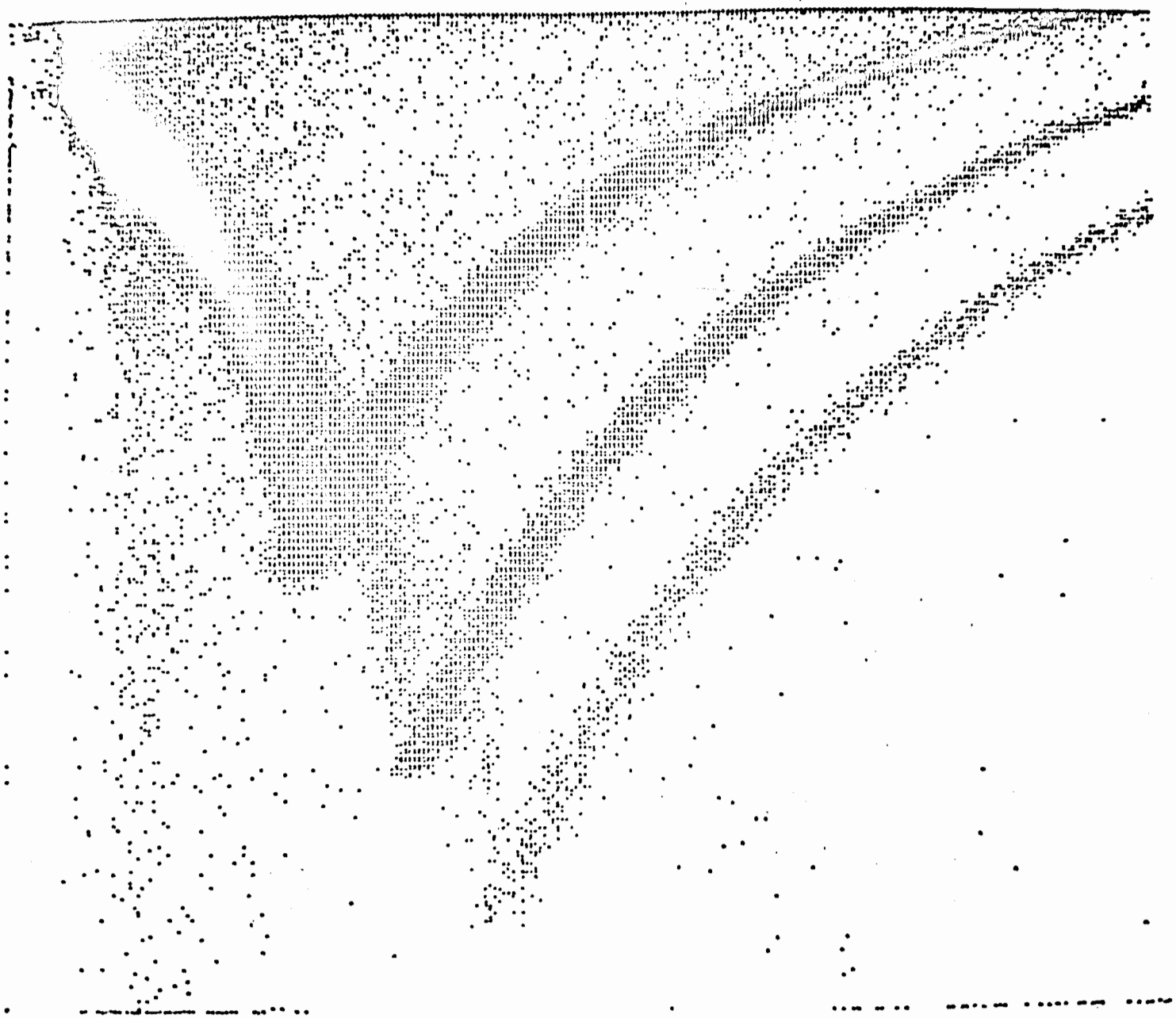

FIG. 3

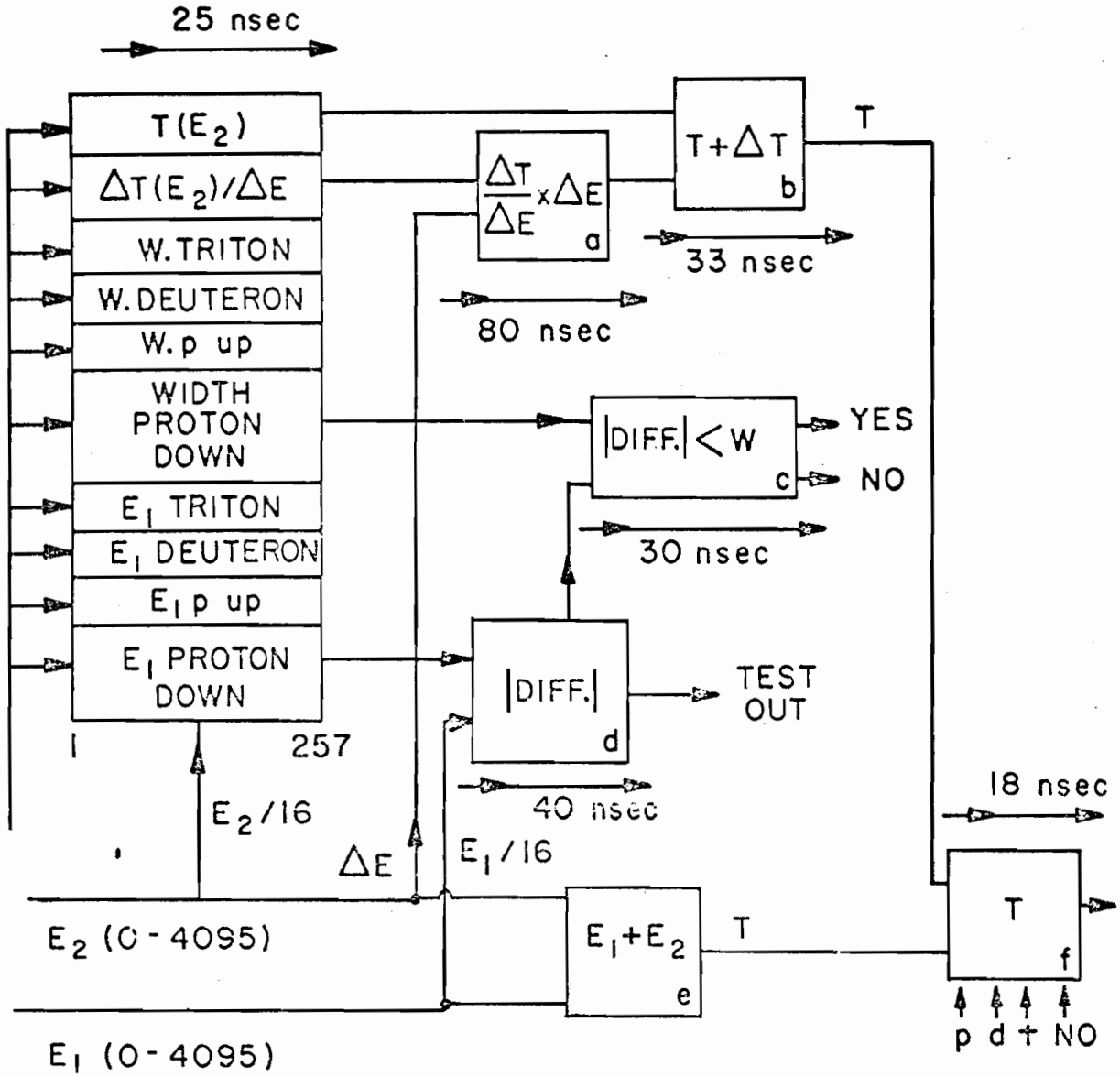


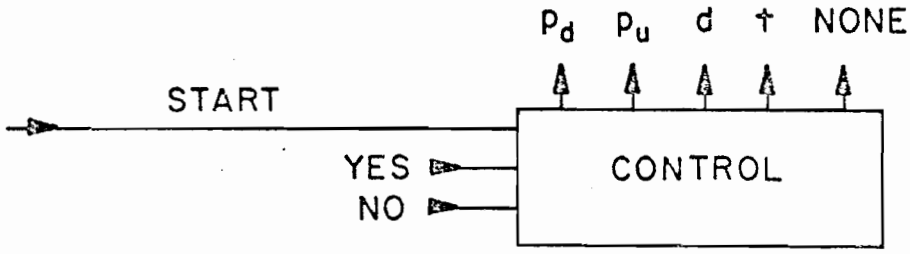


25 + 33 + 18 = 156 nsec

a,b,c,d,e,f ARE SEPARATE ARITHMETIC UNITS

FIG. 4

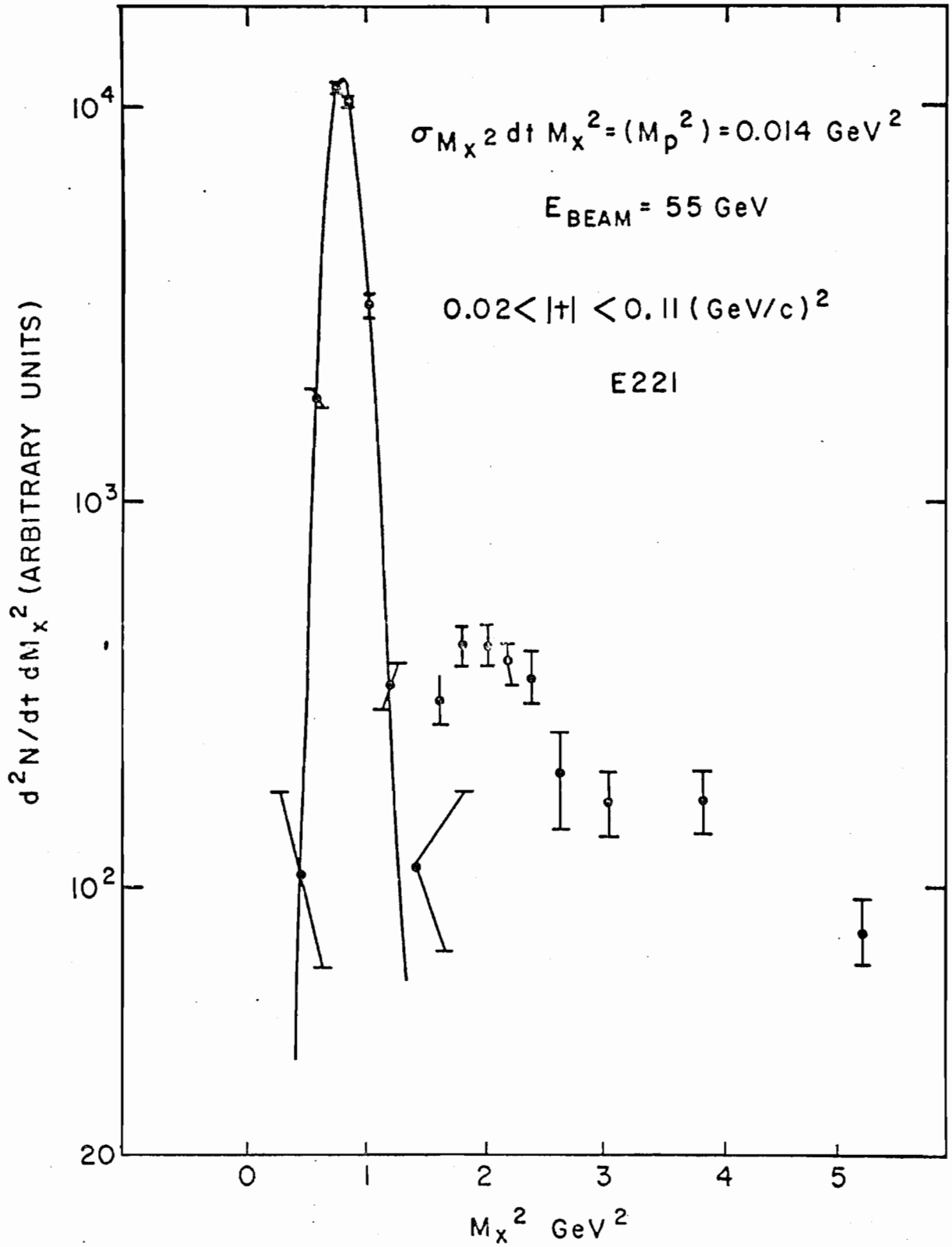
$\sigma_{M_x^2 dt M_x^2} = (M_p^2) = 0.014$ GeV$^2$
$E_{BEAM} = 55$ GeV
$0.02 < |t| < 0.11$ (GeV/c)$^2$
E221
$10^4$
$10^3$
$10^2$
20
0
1
2
3
4
5
$d^2N/dt\,dM_x^2$ (ARBITRARY UNITS)
$M_x^2$ GeV$^2$

FIG. 5

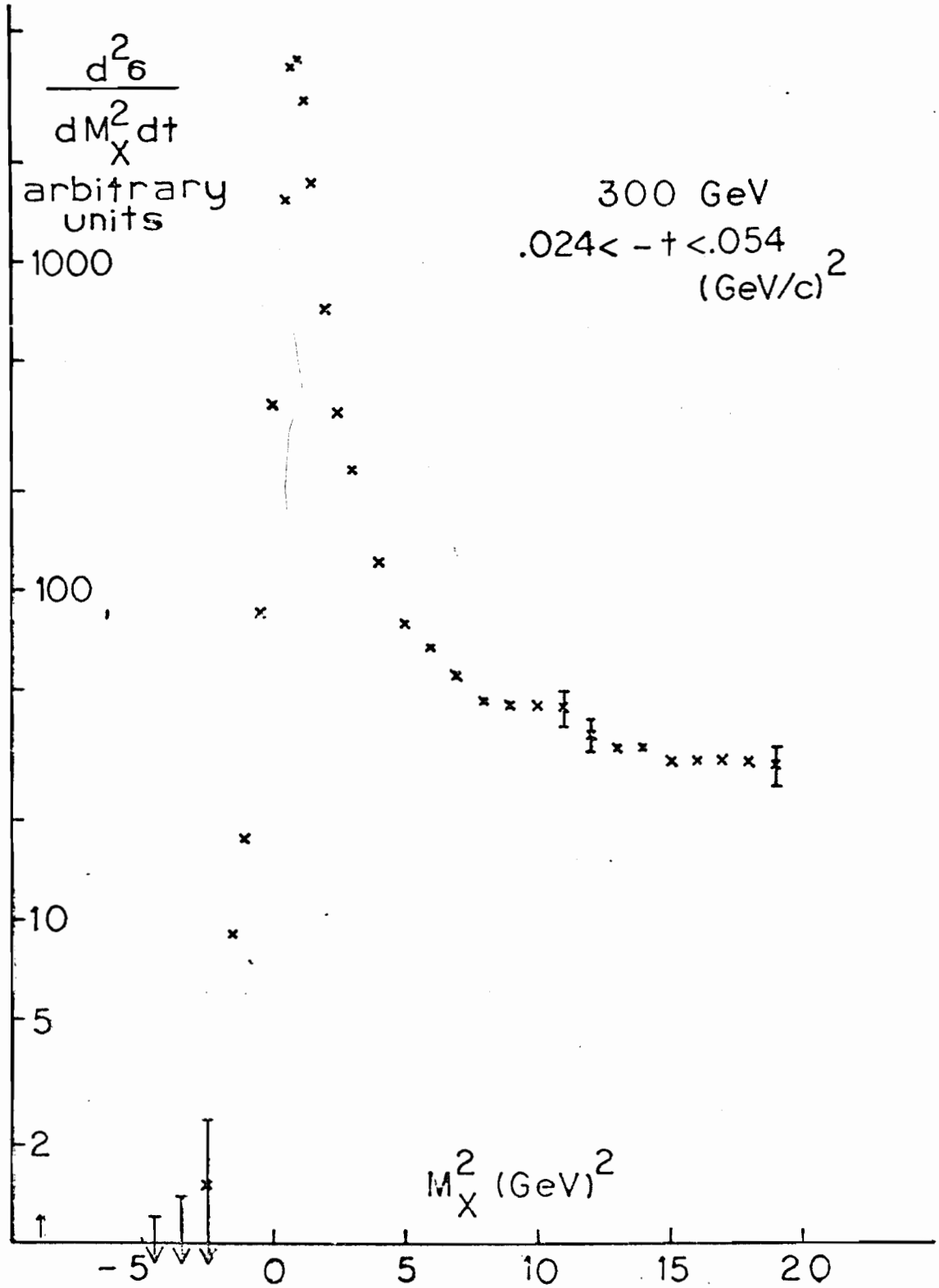
$\frac{d^2\sigma}{dM_X^2 dt}$
arbitrary units
1000
100
10
5
2
300 GeV
.024< −t <.054
(GeV/c)$^2$
$M_X^2$ (GeV)$^2$
−5
0
5
10
15
20

FIG. 6

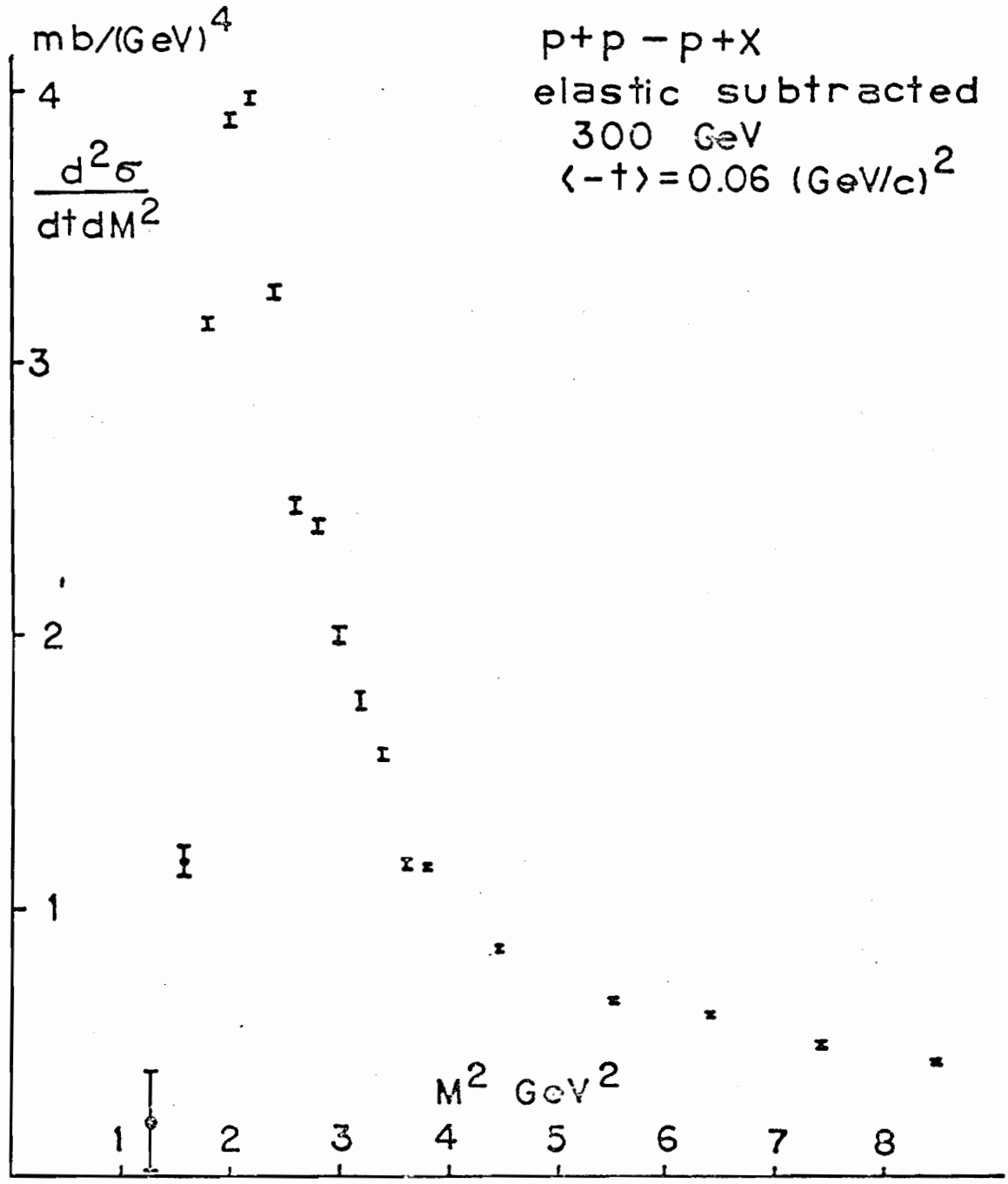
mb/(GeV)$^4$
$\frac{d^2\sigma}{dtdM^2}$
p+p → p+X
elastic subtracted
300 GeV
⟨−t⟩ = 0.06 (GeV/c)$^2$
4
3
2
1
$M^2$ GeV$^2$
1
2
3
4
5
6
7
8

FIG. 7

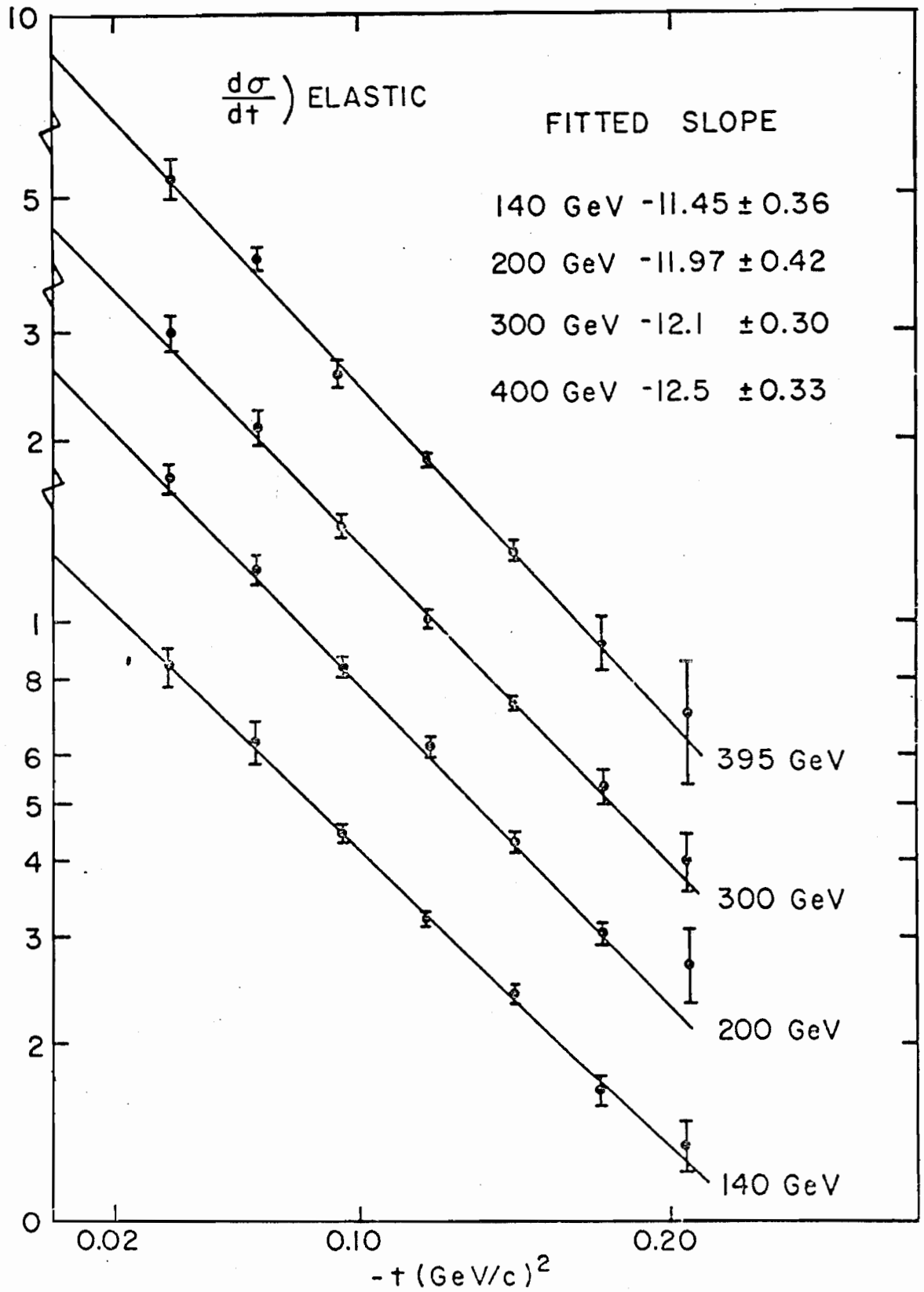
$\frac{d\sigma}{dt}$) ELASTIC
FITTED SLOPE
140 GeV -11.45 ± 0.36
200 GeV -11.97 ± 0.42
300 GeV -12.1 ± 0.30
400 GeV -12.5 ± 0.33
395 GeV
300 GeV
200 GeV
140 GeV
10
5
3
2
1
8
6
5
4
3
2
0
0.02
0.10
0.20
$-t\ (GeV/c)^2$

FIG. 8

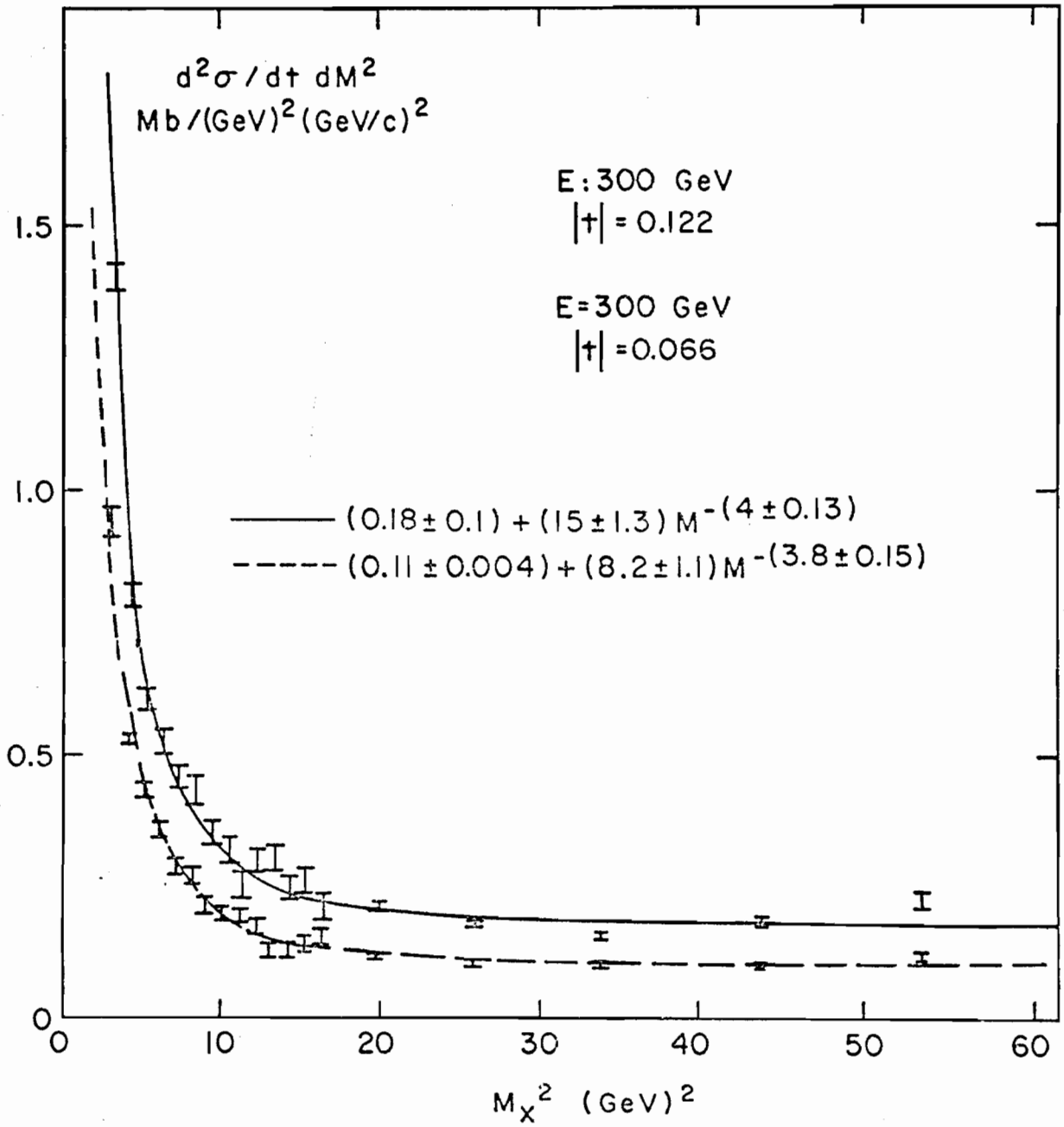
d²σ/dt dM²
Mb/(GeV)²(GeV/c)²
E:300 GeV
|t| = 0.122
E=300 GeV
|t| =0.066
(0.18±0.1) + (15±1.3) M^-(4±0.13)
(0.11±0.004) + (8.2±1.1) M^-(3.8±0.15)
1.5
1.0
0.5
0
0
10
20
30
40
50
60
Mx² (GeV)²

FIG. 9

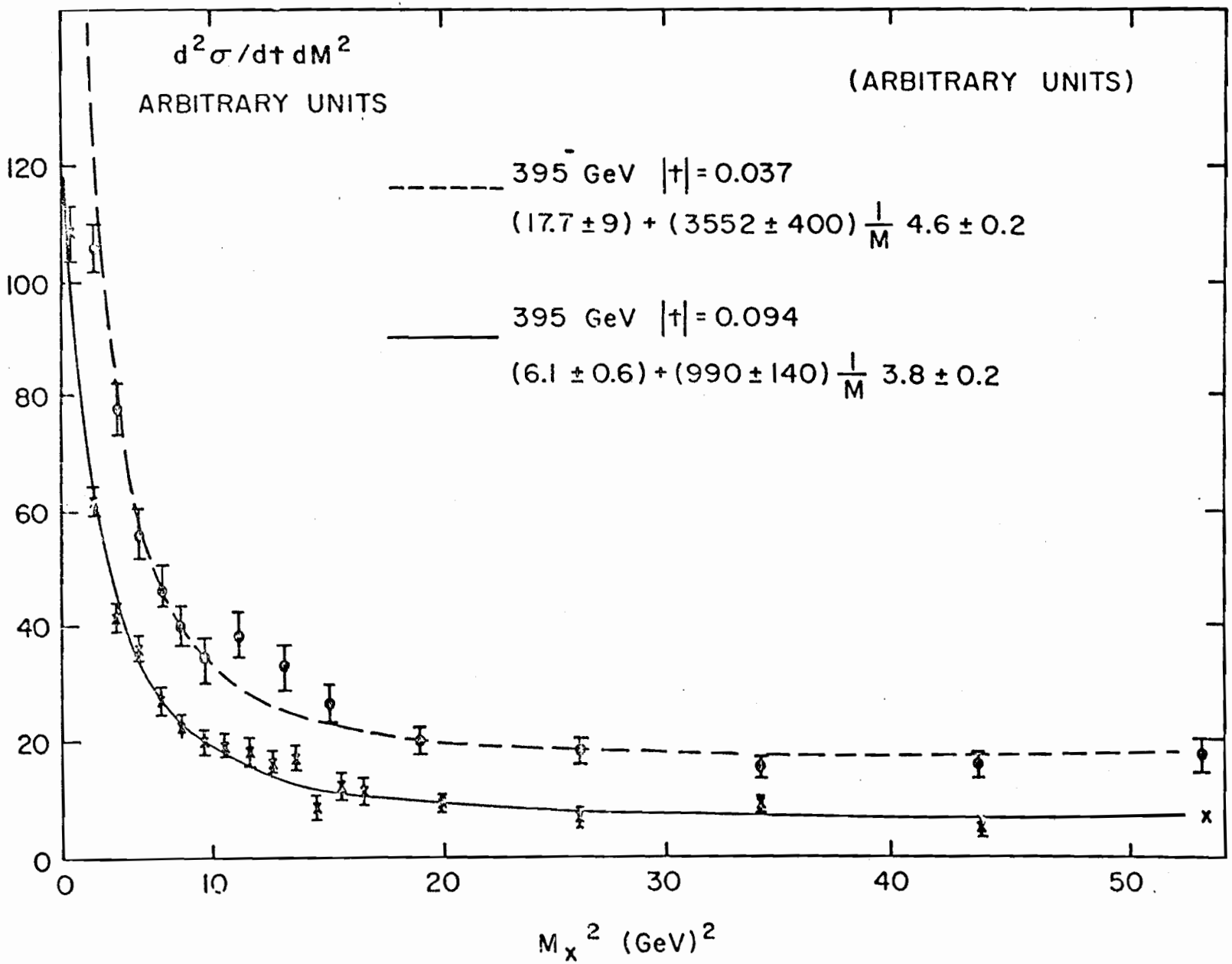
$d^2\sigma/dt\,dM^2$
ARBITRARY UNITS
(ARBITRARY UNITS)
395 GeV $|t| = 0.037$
$(17.7 \pm 9) + (3552 \pm 400)\frac{1}{M}^{4.6 \pm 0.2}$
395 GeV $|t| = 0.094$
$(6.1 \pm 0.6) + (990 \pm 140)\frac{1}{M}^{3.8 \pm 0.2}$
120
100
80
60
40
20
0
0
10
20
30
40
50
$M_x^2$ $(GeV)^2$

FIG. 10

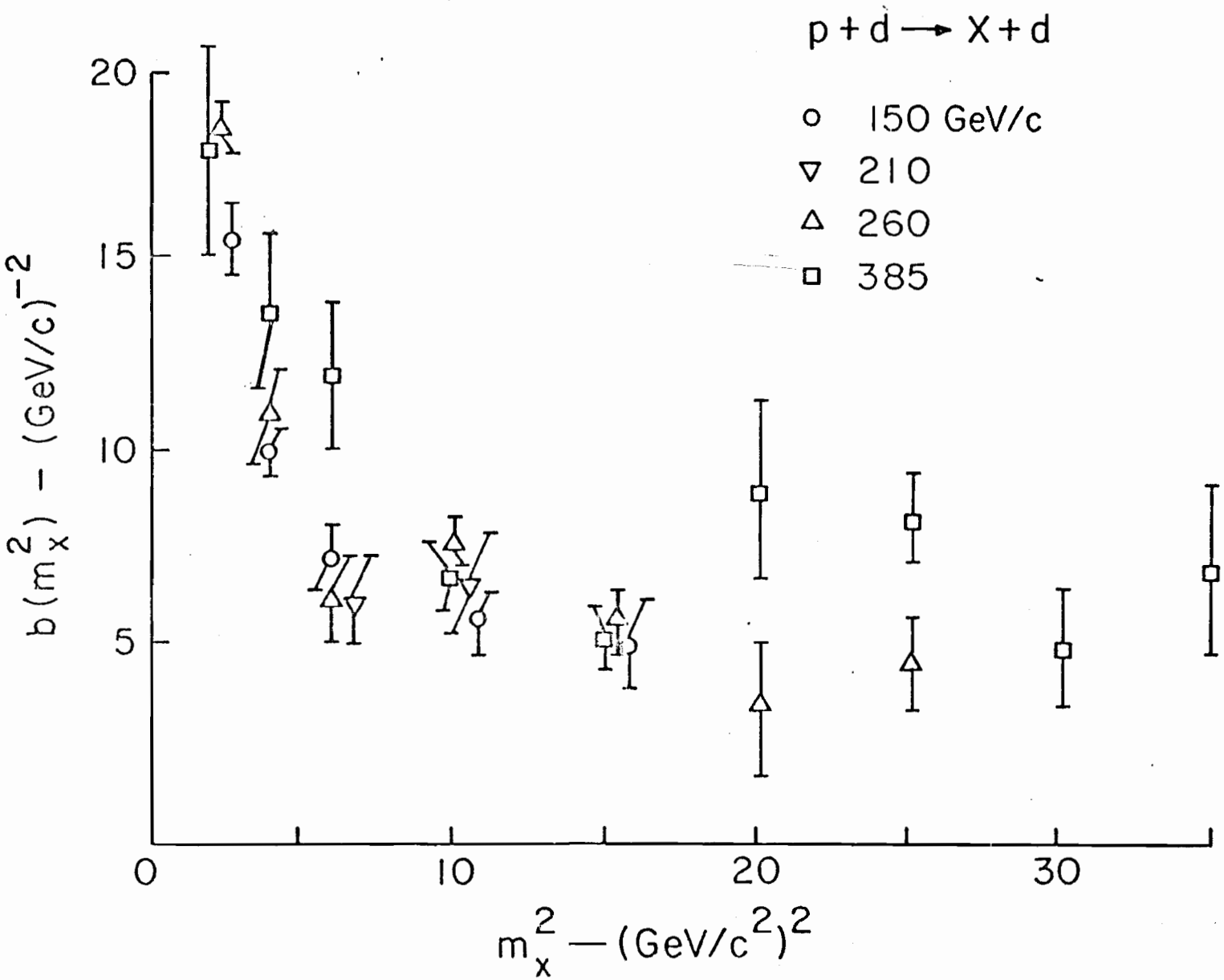
p + d → X + d
150 GeV/c
210
260
385
20
15
10
5
0
10
20
30
b(m²x) – (GeV/c)⁻²
m²x — (GeV/c²)²

FIG. 11

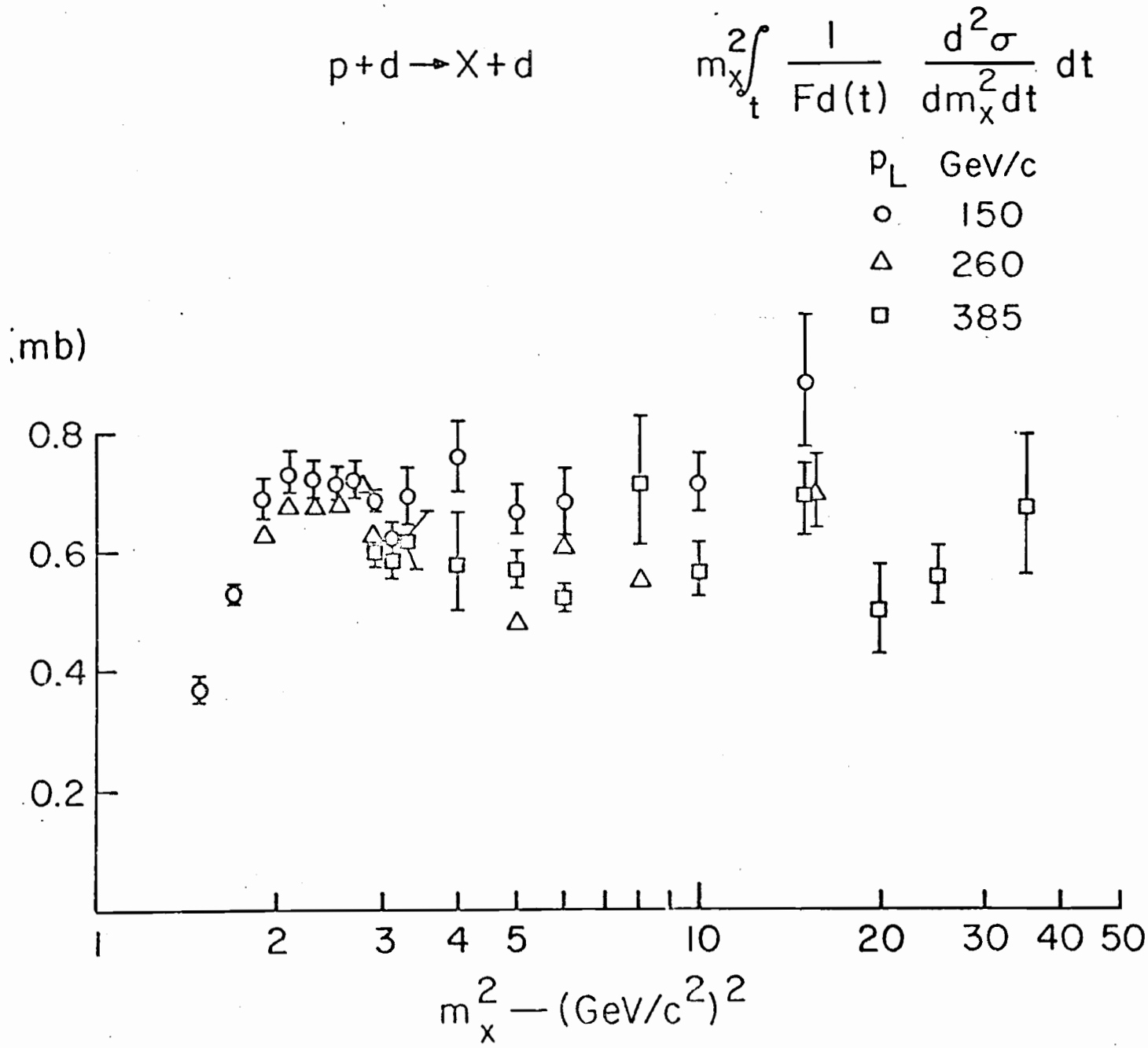
p+d → X+d
$m_x^2 \int_t \frac{1}{Fd(t)} \frac{d^2\sigma}{dm_x^2 dt} dt$
$p_L$ GeV/c
150
260
385
(mb)
0.8
0.6
0.4
0.2
1
2
3
4
5
10
20
30
40
50
$m_x^2$ — $(GeV/c^2)^2$

FIG. 12

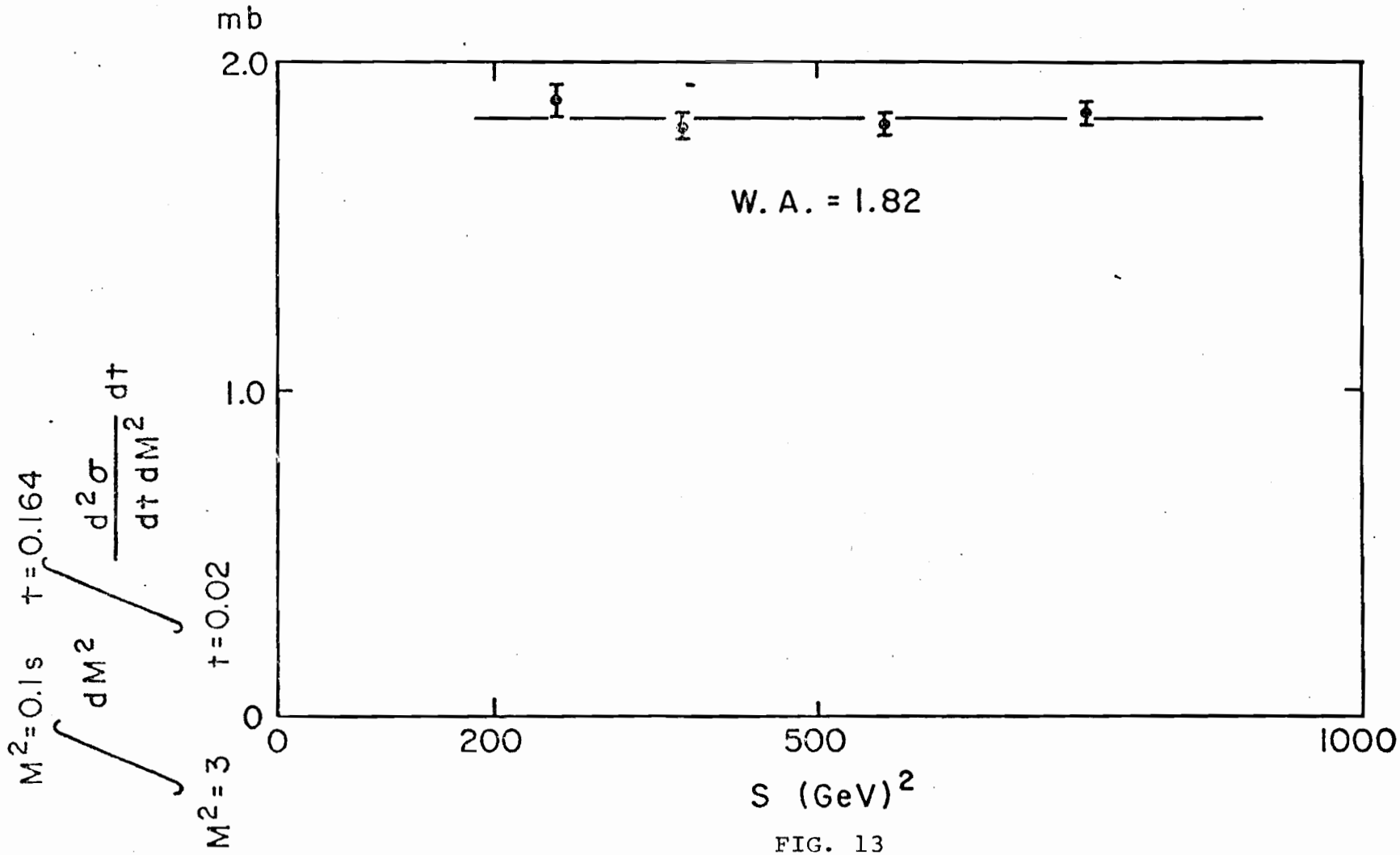
mb
2.0
1.0
0
W. A. = 1.82
0
200
500
1000
S (GeV)$^2$
$\frac{d^2\sigma}{dt\,dM^2}\,dt$
t=0.164
t=0.02
$M^2$=0.1s
$dM^2$
$M^2$=3

FIG. 13